Drift Velocity Calibration of the CLAS Drift Chambers

E.Burtin[a], G.P.Gilfoyle[b], M.V.Kossov[c], M.D.Mestayer[d], L.Y.Murphy[e]

[a]University of South Carolina, Columbia, SC, USA
[b]University of Richmond, Richmond, VA, USA
[c]Christopher Newport University, Newport News, VA, USA
[d]CEBAF, Newport News, VA, USA
[e]CE Saclay, Gif sur Yvette, France

1. Introduction

The CEBAF Large Acceptance Spectrometer (CLAS) is designed to have a momentum resolution in the range $\delta p/p \approx 0.5-1.0\%$ and an angular resolution of about 1.0 *mrad*. In order to achieve these goals the drift chambers must measure tracks with a spatial resolution of 200 μm[1]. The chambers must be calibrated accurately and that calibration must be maintained in the face of variations in running conditions like the atmospheric pressure and temperature of the hall. We have developed techniques for calibrating, monitoring and compensating for variations in the drift velocity of the drift chamber gas due to these changing operating conditions.

The outline of this CLAS Note is as follows. The experimental apparatus is described first and the form of the relationship between the measured drift time and the distance-of-closest-approach of a straight track to a sense wire is presented. Algorithms for determining the maximum drift time, an essential parameter in our characterization of the chamber response, are presented plus a technique for measuring directly the maximum drift time. Finally, the result of compensating for changing conditions is presented.

2. Experimental Details

This study was performed with the Region-3, 'nose cone', prototype chamber in a cosmic-ray telescope (see Figure 1 for a schematic drawing). The prototype reproduces the most-forward-angle portion of the Region 3 drift chambers and contains 192 sense

wires, instead of the 2304 sense wires of an actual chamber, but in other aspects of construction and on-board instrumentation is the same. The chamber has a hexagonal wire arrangement, with sense wires grouped into two six-layer superlayers. For the work described here a 50:50 mixture of Argon-Ethane was used. The chamber was operated with sense, field, and guard wires set at $+1800\ V$, $-900\ V$, and $+643\ V$, respectively. The leakage currents for the sense, field, and guards wires were all in the range $8 - 15\ nA$ during the entire run.

The sense wires were amplified in two stages with a gain of $20\ mV/\mu A$. The amplified signal was discriminated with a Philips 706 module with a threshold set to $10\ mV$. Subsequent analysis of the data (to be presented in a later CLAS Note) leads us to estimate that this threshold corresponds to a minimum detectable signal of three electrons. The discriminator output provided a stop to one of the channels of a LeCroy 2228 TDC module.

Cosmic rays were detected in the chamber with a telescope consisting of two pairs of plastic scintillators placed above and below the chamber. Time jitter occurred in the start signal with a range of $1 - 2\ ns$. This effect was due to variation for different tracks of the propagation time in the scintillator and the time-of-flight of the cosmic ray between the chamber and the scintillators. Data acquisition was done with an array of CAMAC modules and the computer code TRACK [2] running on a MicroVax computer. We fit cosmic ray tracks by minimizing the residual between the calculated distance-of-closest-approach (D) of the fitted track to a wire with the distance from the wire as generated from its drift time (T) alone. In Figure 2 we plot D versus T for wires from one particular layer which was excluded from the track fit. The resulting scatterplot is the familiar drift velocity function.

We will show below that the maximum drift time is one of the important parameters that characterizes the drift velocity function. To make a direct measurement of the maximum drift time we used an ultra-violet laser to induce photo-emission of electrons from a field wire [3]. The apparatus for the test is shown in Figure 3. The photon source was an LN203C nitrogen laser from Laser Photonics delivering $100\ \mu J$/pulse of peak power in $600\ ps$ pulses up to a rate of 50 Hz. The rate is adjustable and the laser was usually run at 1 Hz. The nominal wavelength is $337.1 \pm 0.1\ nm$. This laser employed a thyratron to generate pulses instead of a spark gap used in lasers in previous studies [3,4]. It emits RF noise that can overwhelm the amplified signal from the sense wire that provides the stop signal for the TDC. We were able to reduce this noise below the $10\ mV$ discriminator threshold on the amplified sense-wire signal by several methods. An aluminum box was built to hold the laser with an isolation transformer in the wall of the box and a shielded cable providing power. The bottom and side walls were welded to prevent RF leakage. Long (about 4 inch) tubes were used as attenuating waveguides at each gas and light port to reduce RF leakage. Standard BNC feedthroughs were used to extract a timing signal

from the enclosed laser for monitoring purposes. An RF gasket was attached to the rim of the box where an aluminum lid covered the box. Placing a single lead brick on the lid to hold it firmly in place significantly reduced the RF leakage.

The drift chamber for this part of our investigation was a single cell prototype with a single sense wire, six field wires in a hexagonal arrangement to mimic the CLAS design, and six more guard wires for field shaping. A photodiode placed about 14 cm from the struck wire was used to provide a fast (rise time $\leq$ 1 ns), reference signal as a start for the time-to-digital converter [4]. A quartz lens was used to focus the beam to a spot of dimensions about $1mm \times 1mm$ or less.

We observed a large (pulse height $\geq$ 200mV) signal at the output of the sense-wire signal amplification when the laser beam was directed at a field wire in t[redacted]ingle-cell prototype. In fact, the drift chamber signal was so large it saturated a VPI po[redacted]amplifier that is similar to the ones that will be used in the CLAS. We also directed the laser beam through a mylar window in the side of the nose cone prototype and observed similar behavior when the beam struck a field wire in that chamber. The signals from the photodiode and the drift chamber were collected with the same data acquisition system that was used with the nose cone prototype.

3. The D-T Correlation

In Figure 2 we have indicated the maximum possible drift distance (D_{max}) as well as the corresponding maximum drift time, T_{max}. Shown as different symbols are data points from tracks with an entrance angle of $25° - 30°$ and those with an entrance angle of $0° - 5°$. Clearly, there is a track angle dependence to the D-T correlation. However, note that the two data samples are characterized by the same value of T_{max}.

To understand this effect physically, we present in Figure 4 a plot of isochrones for the cell in question, calculated using the program, GARFIELD [5]. Near the wire, the isochrones are circular, meaning the $D-T$ function is independent of track angle. Further from the wire the isochrones become non-circular, showing track angle dependence. Near the outer edges of the cell the isochrones become hyperboloid. This implies that the first-arriving ions from tracks which are near the periphery of the cell come from the high-field region near the field wire regardless of the location of the point at which the track is closest to the wire. This is the reason that the same value of T_{max} applies to tracks of any angle. For example, the two tracks shown (at 0° and 30°) have different distances of closest approach but give the same value for the time of the first arriving drift electron.

Looking again at Figure 2, we note two other features of the data. First, the slope at small values of time is approximately equal to the slope at the maximum drift time (T_{max}). Second, an inflection point (which corresponds to a minimum in the drift velocity) occurs at a distance of $\approx$0.615 of the maximum distance. The precise location of the inflection

point was obtained from our GARFIELD simulation discussed below.

These observations led us to a polynomial expression for the D vs. T function for a particular entrance angle θ with only three adjustable parameters, V_0 (the saturated drift velocity), T_{smear} (the time smearing for tracks near the wires due to discrete ionization), and T_{max} (the maximum drift time). The quantities V_0 and T_{smear} are roughly constant, thus when some operating condition varies (like drift chamber gas pressure), we can characterize the change in the drift velocity with one parameter, T_{max}.

We now investigate the functional form for the dependence of D on drift time. We first derive the function for the case of $\theta = 30°$, *i.e.* where the track is perpendicular to a line joining sense and field wire. For simplicity, we assume a simple three-power form, the first term of which is linear.

$$D = V_0 \cdot T + b \cdot ((\frac{T}{T_{max}})^n + c \cdot (\frac{T}{T_{max}})^m) \quad .$$

The quantity V_0 is the value for the saturated drift velocity near $T = 0$, and T_{max} is the maximum drift time.

The first constraint is that the drift velocity near the sense wire ($T = 0$) is equal to the drift velocity near the field wire ($T = T_{max}$). Even though the field wire's local electric field at some particular distance is half that for the sense wire, the local drift velocities are approximately equal because this is in the high electric field region where drift velocities saturate. Therefore

$$\frac{dD}{dT}(T = 0) = \frac{dD}{dT}(T = T_{max})$$

or

$$V_0 = V_0 + b \cdot (n + c \cdot m) \quad .$$

Thus,

$$c = -n/m \quad .$$

The second constraint is that the drift velocity reaches a minimum at the point of minimum electric field strength. Along a line from sense to field wire, we determined that the electric field reaches a minimum at approximately 0.615 of the distance from sense to field wire, using the GARFIELD program. The number 0.615 is characteristic of an infinite grid of hexagonal cells which our chambers approximate. It does not depend on cell size or voltage. In terms of drift time, this inflection point occurs at $T \approx 0.605 \cdot T_{max}$, for our particular running conditions. The value 0.605 is not a geometrical constant but is approximately constant for our choice of operating voltage. Therefore,

$$\frac{d^2D}{dT^2}(T = 0.605 \cdot T_{max}) = 0 \quad .$$

So

$$n \cdot (n-1) \cdot 0.605^n = c \cdot m \cdot (m-1) \cdot 0.605^m \quad .$$

Substituting $c = -n/m$ yields

$$(n-1) \cdot (0.605)^n = (m-1) \cdot (0.605)^m \quad .$$

Graphically we determined that the equation

$$n = 2.85 - 0.65 \cdot (m-3)^{0.7}$$

describes the solution set. Using this relation between n and m, we were able to fit the $D-T$ data to the functional form to obtain $n = 2$ and $m = 4.5$ as the exponents which best fit the data. To obtain good agreement with data, it was also necessary to add an asymmetric time smearing for small times due to the finite ion deposition density along the track.

We then fixed the values of n and m at 2 and 4.5 respectively, and assumed that changes to the drift velocity function could be characterized by a changing value of V_0 or b. By noting that the maximum drift distance, D_{max}, occurs at time, T_{max}, we are able to express b as follows

$$b = \frac{D_{max} - V_0 \cdot T_{max}}{1 - n/m} \quad .$$

The dependence on the entrance angle of the track is incorporated in D_{max}, the distance from the sense wire to the perimeter of the cell along a line perpendicular to the track. In other words,

$$D_{max} = D_{cell} \cdot \cos(30^\circ - \theta)$$

where D_{cell} is the distance from the sense wire to a field wire. So, we have parameterized the drift distance in terms of two fundamental parameters, V_0, the saturated drift velocity, and T_{max}, the maximum drift time.

We note here that we also explored the use of an arbitrary polynomial to characterize the $D-T$ function. After trying several different forms we settled on the function

$$T = a_1 + a_2 T + a_3 T^2 + T^3(a_4 + a_5 \tan(\theta))$$

where θ is the entrance angle of the track. Analysis of our data with this function produced essentially the same distribution of residuals as the previous function.

Our calibration strategy will rely on assuming that changes to the drift velocity correlation can be adequately described as a change to a single parameter, T_{max}, which we must determine and periodically update in a calibration file. We will present our implementation of this strategy below, but first we discuss methods to determine T_{max}.

4. Measuring T_{max}

We have explored several techniques to determine the maximum drift time, but first we must precisely define T_{max}. One naively expects T_{max} to be the drift time for tracks whose distance of closest approach lies near the field wire, the farthest geometric point from the sense wire. However, recall the discussion above explaining why tracks with different entrance angles near the periphery of the cell will generate the same drift time. The topology of the isochrones in this region is complex; they shift from a hexagonal shape to a hyperboloid one over a small distance. In turn, the discrete nature of the ionization produced by a track means that clusters will be generated, on average, every 300 μm. Hence, two identical tracks can produce ion clusters that lie on different isochrones. The topology of the isochrones leads to a 'smearing' of drift times at large distances from the sense wire. A typical drift time spectrum for a single layer is shown in Figure 5. Notice that at large times the edge is not sharp, but drops to zero over a range of about 100 ns. We have defined the maximum drift time, T_{max}, as the midpoint of the region of the dropoff.

We now discuss several methods for determining the maximum drift time from our data. In the region of the large-time edge, the slope of the data should pass through a maximum at T_{max}. One can calculate this slope from one bin to the next and locate the maximum. However, this method suffers from inadequate statistics in the region of interest. The number of counts is dropping rapidly and one must take the difference between two small numbers. This procedure has a large uncertainty that makes it unusable.

We fit the drift distance versus drift time spectrum (the $D - T$ distribution) with the functional form discussed above. This method is biased because it depends on the track-fitting algorithm. The current value of the distance-of-closest-approach (D) depends upon the parameters of the correlation function used to calculate D from the drift time T. This procedure is thus inherently an iterative and time-consuming one.

We also fit the large-time edge of the drift time spectrum with a function of the form

$$N = \frac{N_0}{1 + exp[(T - T_{max})/a]}$$

where N_0 is a normalization factor, T is the drift time, and a is the width of the drop-off region. One must choose a low-time cutoff to avoid 'distorting' the fit with the large peak in the drift time spectrum at small times (the cutoff is about 260 ns in Figure 5). Nevertheless, the fit results are insensitive to the choice of this cut-off over a wide time range (200-400 ns for Figure 5) and are consistent with the fits to the $D - T$ distribution. Hence, this method is robust and accurate and has a distinct advantage over the previous method because it is independent of track fitting. It does not depend on the particular form of the function used to calculate the distance-of-closest-approach. However, the large-time-edge fit relies on collecting an accurate drift time spectrum. In the CLAS (as opposed

to the nose cone prototype) the drift time measurement will require a substantial amount of analysis to convert raw TDC readings into drift times because the CLAS will have a common-stop system with a trigger formation time jitter of about 40 ns. Hence, fitting the large-time-edge of the drift time spectrum is a promising technique, but it relies on an 'analyzed' quantity.

Finally, we measured the maximum drift time in a separate test chamber held at the same voltage, pressure, and gas mixture as the nose cone prototype drift chamber. The results are shown in Figure 6. It is a time histogram from a cosmic-ray run on the one-cell chamber. Superimposed upon the continuous distribution of drift times obtained from the cosmic rays are two sharp peaks. The first is the time recorded from the photodiode placed about 14 cm from the field wire illuminated by the laser light and corresponds to the time at which the laser struck the wire (within ≈ 300 ps). The second peak corresponds to electrons emitted from the field wires. The photodiode gives a prompt signal, so we have added one time offset to the two laser peaks in order to align the diode peak with the leading edge of the cosmic ray distribution. The ionization from the wire surface far exceeds the laser's ionization of the gas itself so the difference between the two sharp peaks is a direct measure of T_{max}, the time interval for an electron emitted from a field wire to reach the sense wire. Note that the time difference between the peaks is the same as the over-all time spread of cosmic-ray events, indicating that the laser-induced, photo-emission method correctly measures the parameter T_{max}. This laser calibration method is consistent with the other methods and has the advantage that it can be done independently of any data analysis.

5. Environmental Compensation

We mentioned above that our strategy for maintaining the drift velocity calibration depended on the maximum drift time. To test this idea we collected data over a long (4-day) period during which the atmospheric temperature and pressure varied significantly. We determined the maximum drift time, T_{max}, as a function of the elapsed time of the run, $T_{elapsed}$, using the fit to the large-time edge of the drift time spectrum described above. The results are shown in the upper panel of Figure 7. Notice that the maximum drift time is constant for the first two days or so of the run and then begins to increase significantly (from ≈ 490 ns to ≈ 560 ns) for $T_{elapsed} > 4600$ min. We then optimized the parameters of the drift distance - drift time ($D - T$) function during these first two days of the run when T_{max} was stable. During this time period ($T_{elapsed} < 4600$ min) the resolution in the central region of the cell between the sense and field wires was about 190 μm. This calibration of the $D - T$ function made for the early part of the run was used throughout the rest of the run. The spatial resolution of the nose cone prototype as a function of the elapsed time was determined from the width of a Gaussian fit to the residual of the

excluded layer. The result is shown in the lower panel of Figure 7. For early times the resolution stays near its optimized value of about 200 μm, but for $T_{elapsed} > 4600\ min$ the resolution deteriorates rapidly implying the need to update the calibration of the $D - T$ function. More importantly, this deterioration is precisely correlated with the change in T_{max} shown in the upper panel.

What caused these effects? Because the chamber has a flexible gas bag and operates at atmospheric pressure, we suspected changes in atmospheric pressure were the dominant cause of changes to the drift velocity and of the degraded resolution. To test this idea, we recorded the pressure inside the chamber during the same 4-day run. The results are shown in the upper panel of Figure 8. For comparison we reproduce the time-dependence of the resolution shown in Figure 7. During the early part of the run the pressure changes significantly when the resolution is stable (recall from Figure 7 that the maximum drift time is also constant during this period). For $T_{elapsed} > 4600\ min$ the pressure drops and then increases again while the resolution deteriorates. The time dependence of the atmospheric pressure and the resolution are only imperfectly correlated. This imperfection points to the effect of other additional factors like temperature or gas mixture as sources of changes in the drift velocity. Nevertheless, the precise correlation of the resolution with the maximum drift time supports our strategy of monitoring T_{max} and compensating for changes in this parameter.

We implemented our strategy by measuring T_{max} from the fit to the large-time edge of the drift time spectrum and updating its value in a calibration file. Figure 9 shows our results. We display the average residual between tracks and individual hits plotted versus the distance of the track from the wire. The open circles represent the residual distribution for the large-elapsed-time portion of the run, using a $D - T$ function which gave good resolution ($\approx 200\ \mu m$) for the early part of the run. The resolution had clearly deteriorated. The solid circles represent the residuals during the same time period obtained when the $D - T$ function was corrected for the changing values of T_{max} shown in Figure 7. The minimum in the central region of the cell has returned to about 200 μm. This is our primary result: by measuring and adjusting a single parameter (T_{max}) we are able to keep the drift chambers calibrated in spite of changing environmental conditions.

6. Conclusions

We have discovered that the maximum drift time is a useful parameter that can describe the response of the CLAS drift chambers. It is tightly correlated with changes in the resolution of the nose cone prototype due to changing operating conditions. We have developed a technique to measure T_{max} using the measured drift-time spectrum and to directly measure T_{max} by shining a UV laser on a field wire and determining the drift time of the emitted electrons. Finally, we have demonstrated that one can maintain the

calibration of the drift chambers by updating the value of T_{max} in a calibration file.

References

[1] 'Conceptual Design Report - Basic Experimental Equipment', CEBAF, April 13, 1990.

[2] S.Zhou and R.T.Edwards, 'The CLAS Drift Chamber Track System', CLAS-NOTE-91-001.

[3] R.A.Miskimen and K.Wang, 'Prospects for Drift Chamber Calibration Using a Nitrogen Laser', CLAS-NOTE-91-002.

[4] E.S.Smith and R.Jacobs, 'Photomultiplier Tests for the CLAS TOF', CLAS-NOTE-91-003.

[5] GARFIELD has been developed at the University of Mainz by R. Veenhof and revised by M. Guckes and K. Peters. See HELIOS note 154 (1986).

Figure Captions

1. A schematic drawing of the nose cone prototype.
2. Distance-of-closest-approach (D) versus drift time (T). The light points are for tracks with entrance angles in the range $\theta = 25° - 30°$. The dark crosses are for tracks with entrance angles in the range $\theta = 0° - 5°$. The maximum distances-of-closest-approach for these two angular ranges are indicated by the arrows. The dashed line represents the maximum drift time, T_{max}, derived from a fit to the large-time edge of the drift time spectrum.
3. A schematic drawing of the apparatus used to measure the maximum drift time.
4. Drift Lines and Drift Isochrones (100 ns contours): Region 3 Cell.
5. Drift time spectrum from a Region 3 cell.
6. Results of laser measurement of the maximum drift time. The narrow peak at small time is the reference signal from the photodiode. The narrow peak at large time is from the single-cell drift chamber. The histogram is cosmic ray data collected during the course of one day.
7. Time dependence of the maximum drift time and the resolution in the nose cone prototype.
8. Time dependence of the gas pressure in the nose cone prototype and the resolution of the drift chamber.
9. The dependence of the resolution on the distance-of-closest-approach (D) before and after correction for changing T_{max}.

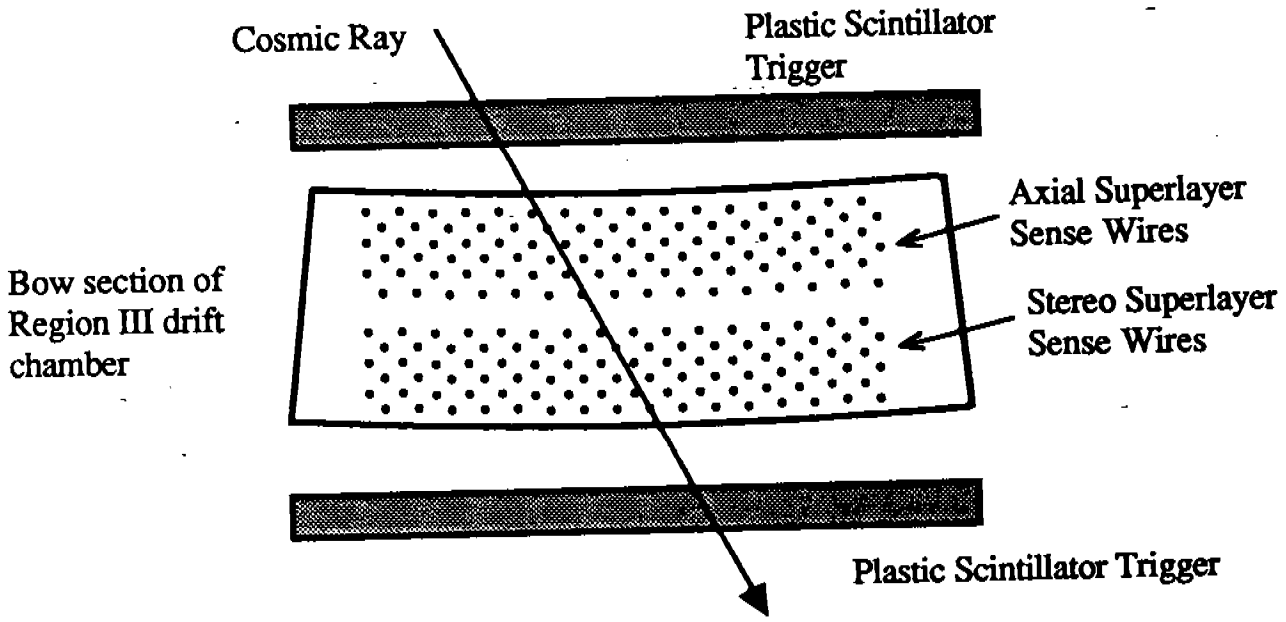
Cosmic Ray
Plastic Scintillator Trigger
Axial Superlayer Sense Wires
Stereo Superlayer Sense Wires
Bow section of Region III drift chamber
Plastic Scintillator Trigger

Figure 1.

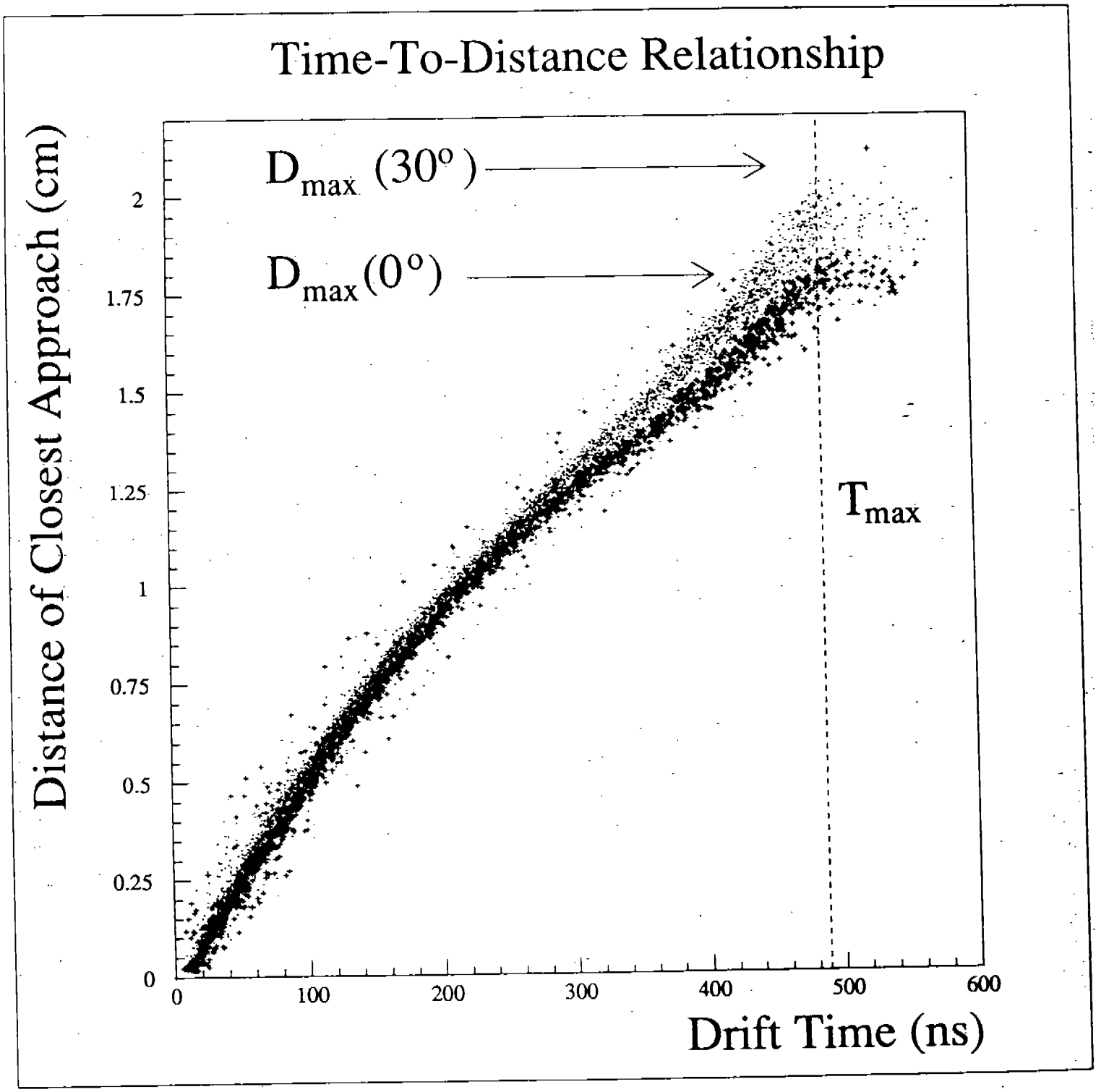
Time-To-Distance Relationship
Distance of Closest Approach (cm)
Drift Time (ns)
D_{max} (30°)
D_{max} (0°)
T_{max}
0
0.25
0.5
0.75
1
1.25
1.5
1.75
2
0
100
200
300
400
500
600

Figure 2.

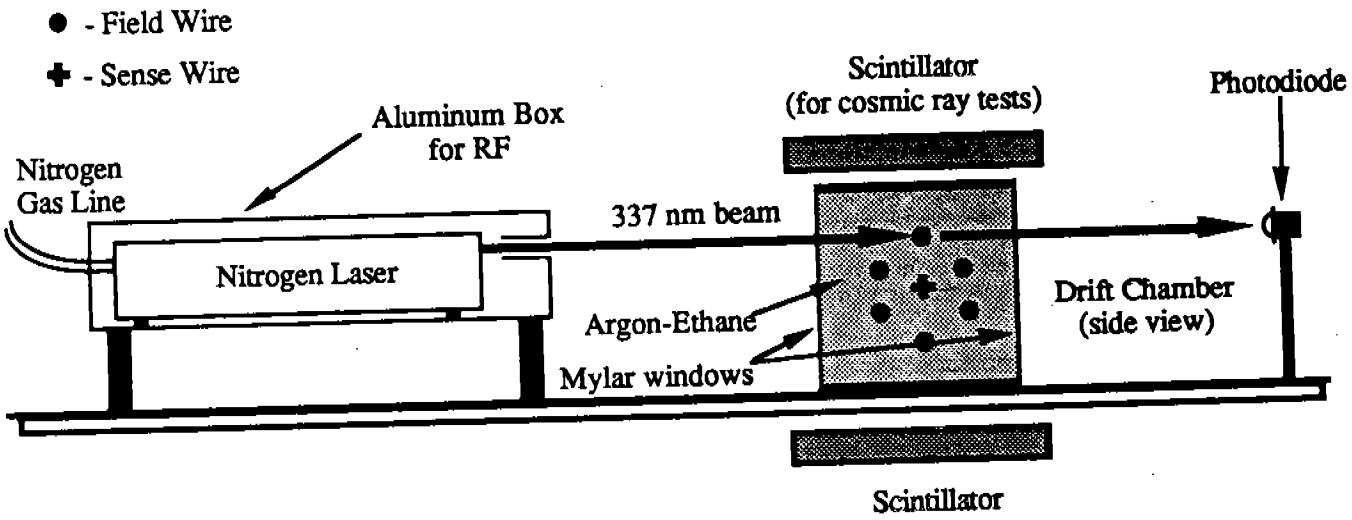
● - Field Wire
✚ - Sense Wire
Aluminum Box
for RF
Scintillator
(for cosmic ray tests)
Photodiode
Nitrogen
Gas Line
337 nm beam
Nitrogen Laser
Drift Chamber
(side view)
Argon-Ethane
Mylar windows
Scintillator

Figure 3.

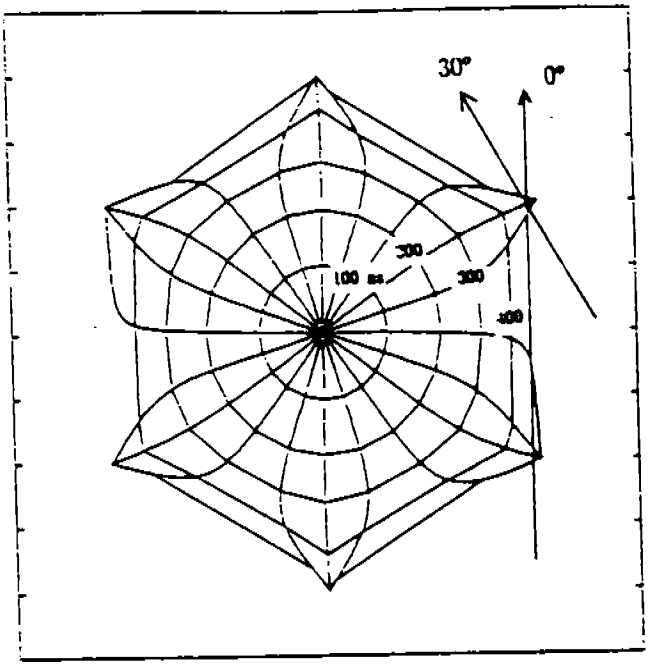

Figure 4.

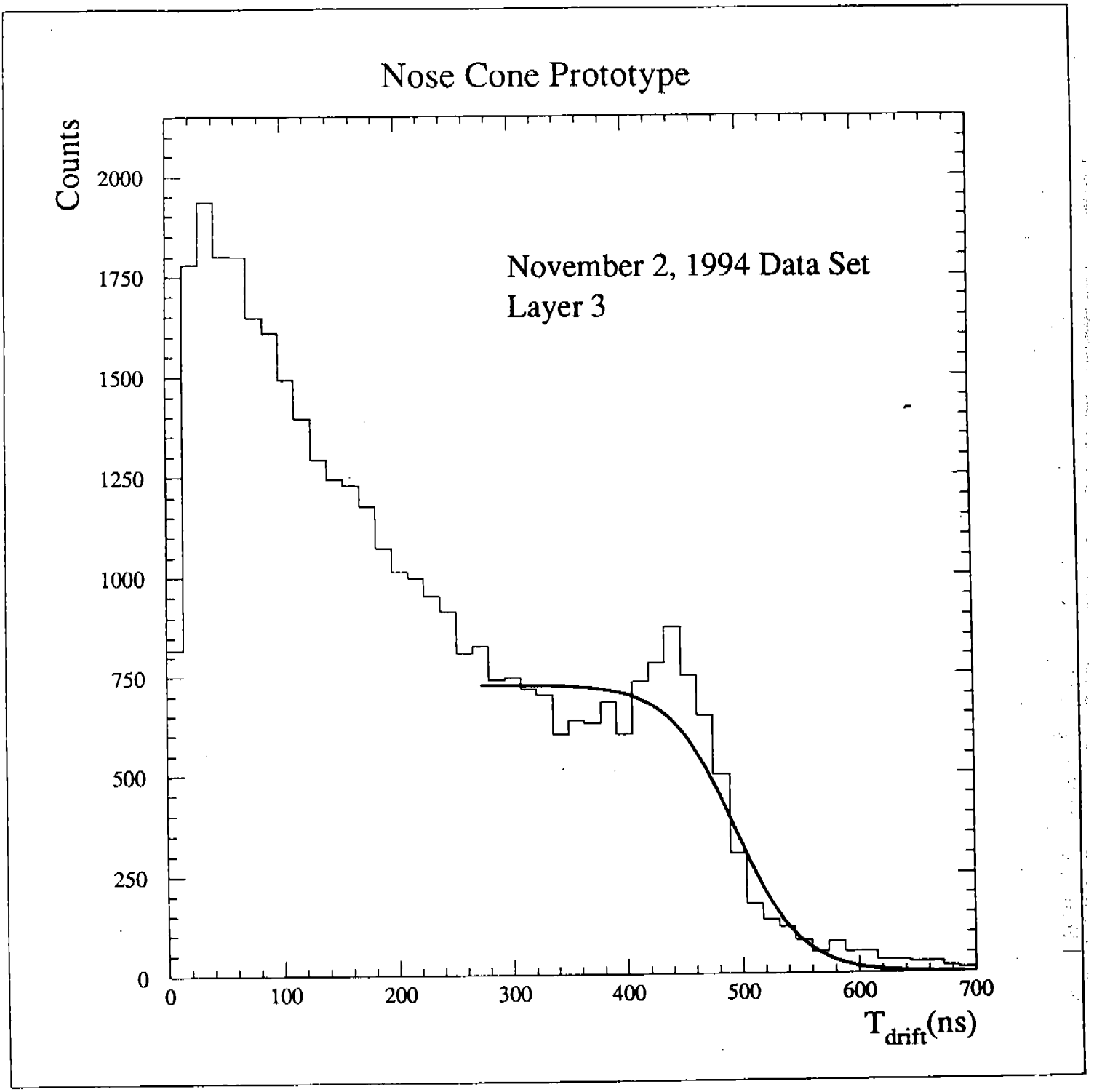
Nose Cone Prototype
Counts
2000
1750
1500
1250
1000
750
500
250
0
November 2, 1994 Data Set
Layer 3
0
100
200
300
400
500
600
700
T drift (ns)

Figure 5.

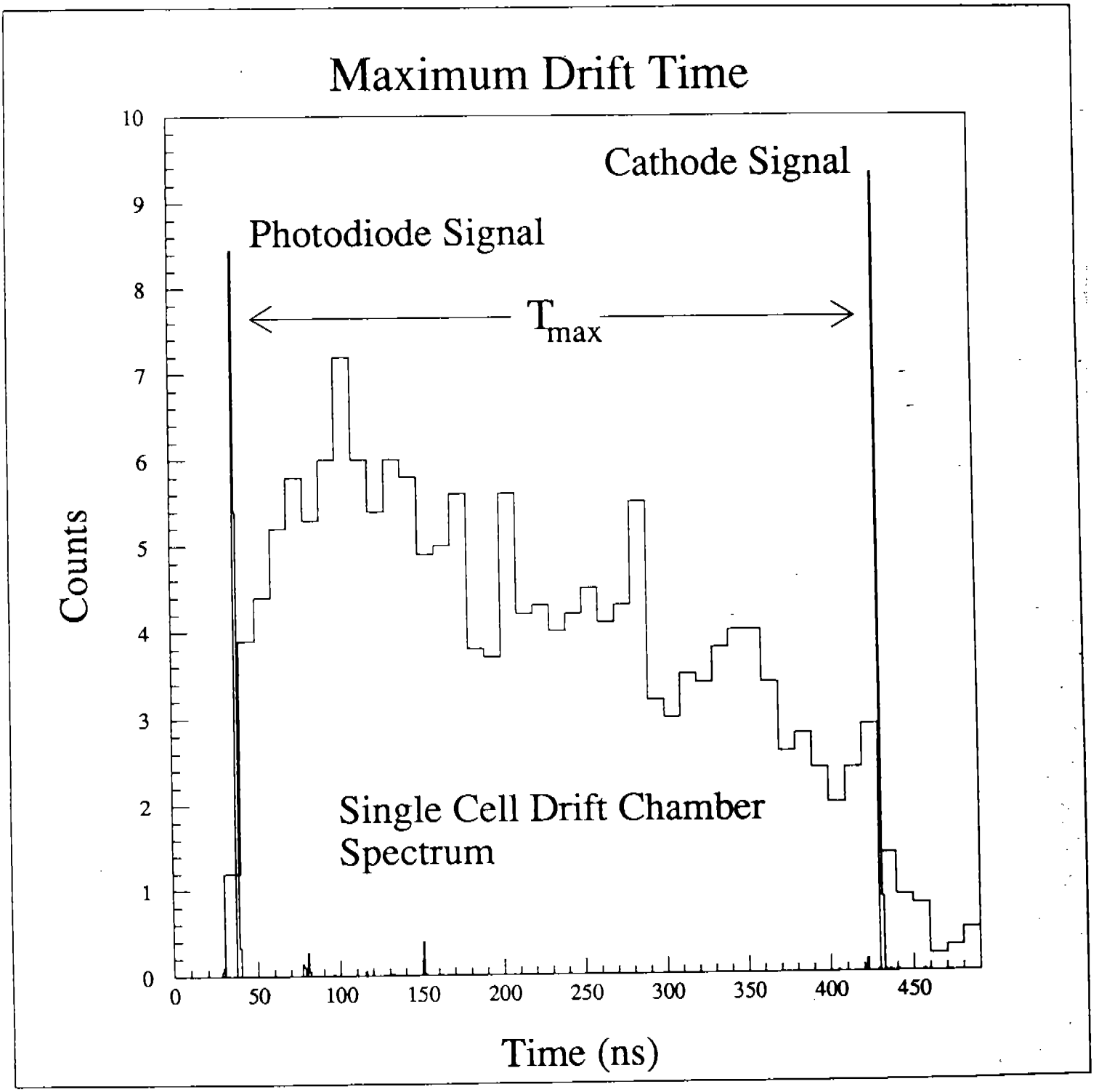
Maximum Drift Time
Cathode Signal
Photodiode Signal
T_{max}
Single Cell Drift Chamber
Spectrum
Counts
Time (ns)
0
1
2
3
4
5
6
7
8
9
10
0
50
100
150
200
250
300
350
400
450

Figure 6.

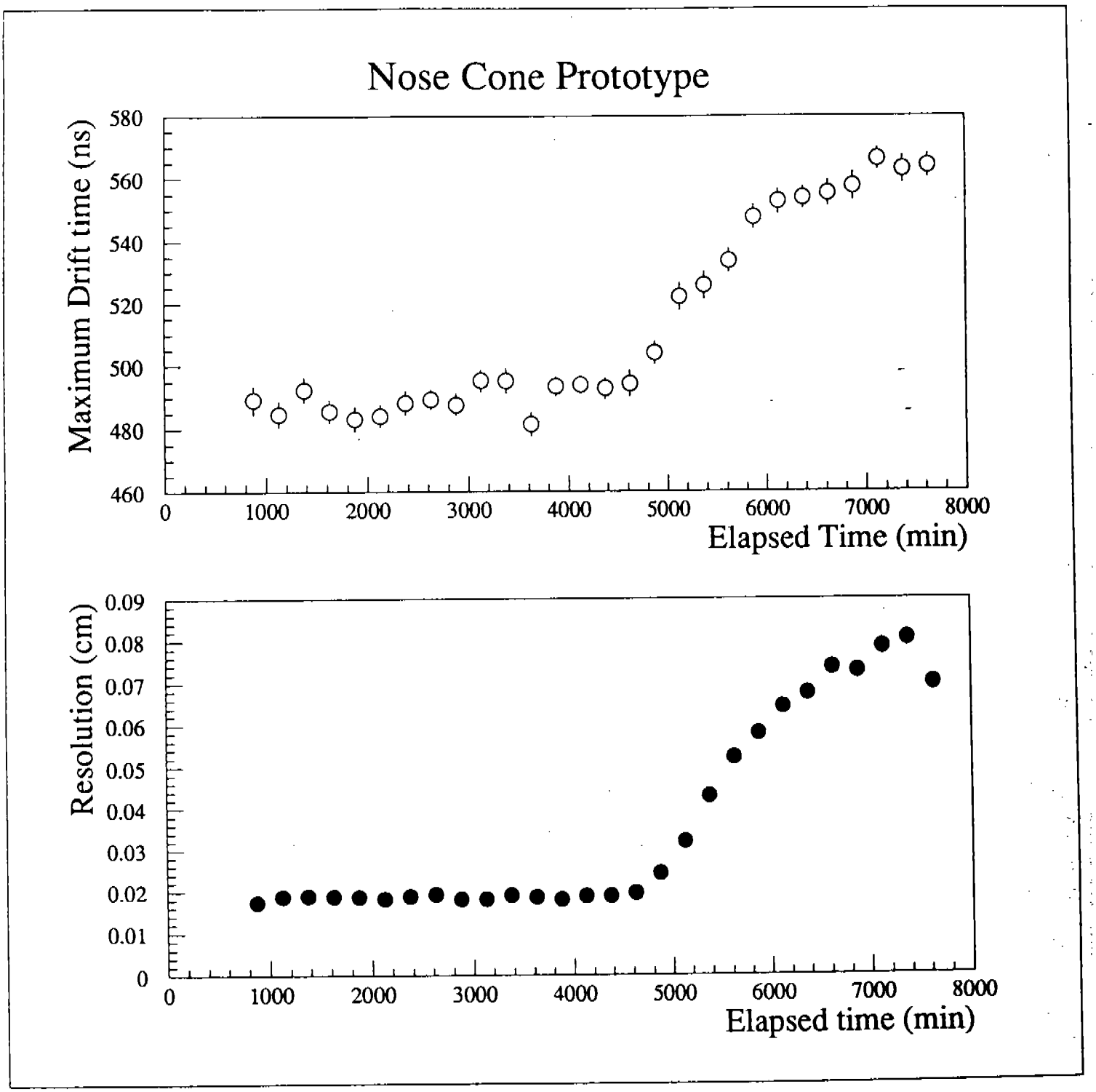
Nose Cone Prototype
Maximum Drift time (ns)
580
560
540
520
500
480
460
0
1000
2000
3000
4000
5000
6000
7000
8000
Elapsed Time (min)
Resolution (cm)
0.09
0.08
0.07
0.06
0.05
0.04
0.03
0.02
0.01
0
0
1000
2000
3000
4000
5000
6000
7000
8000
Elapsed time (min)

Figure 7.

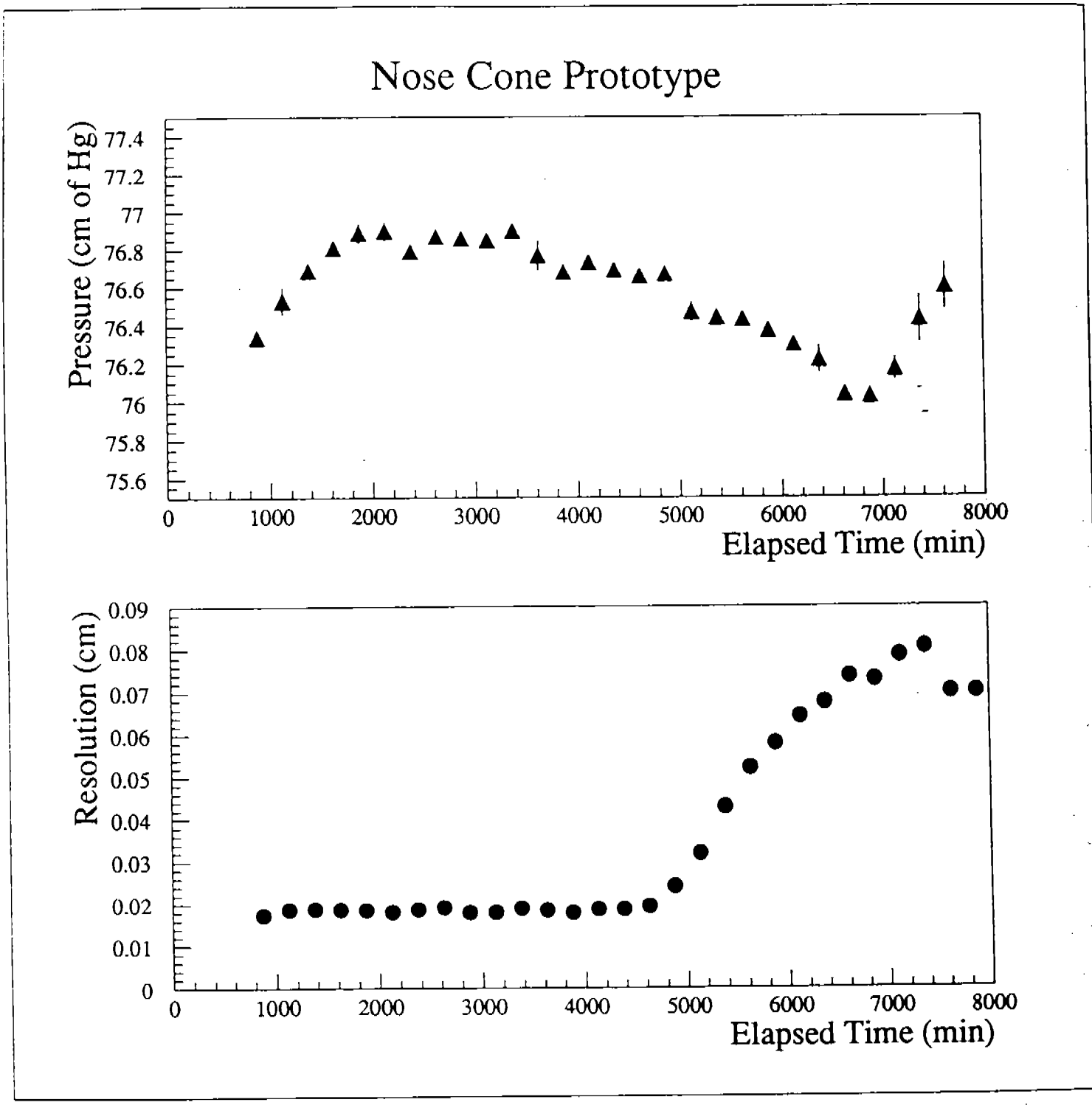
Nose Cone Prototype
Pressure (cm of Hg)
77.4
77.2
77
76.8
76.6
76.4
76.2
76
75.8
75.6
0
1000
2000
3000
4000
5000
6000
7000
8000
Elapsed Time (min)
Resolution (cm)
0.09
0.08
0.07
0.06
0.05
0.04
0.03
0.02
0.01
0
0
1000
2000
3000
4000
5000
6000
7000
8000
Elapsed Time (min)

Figure 8.

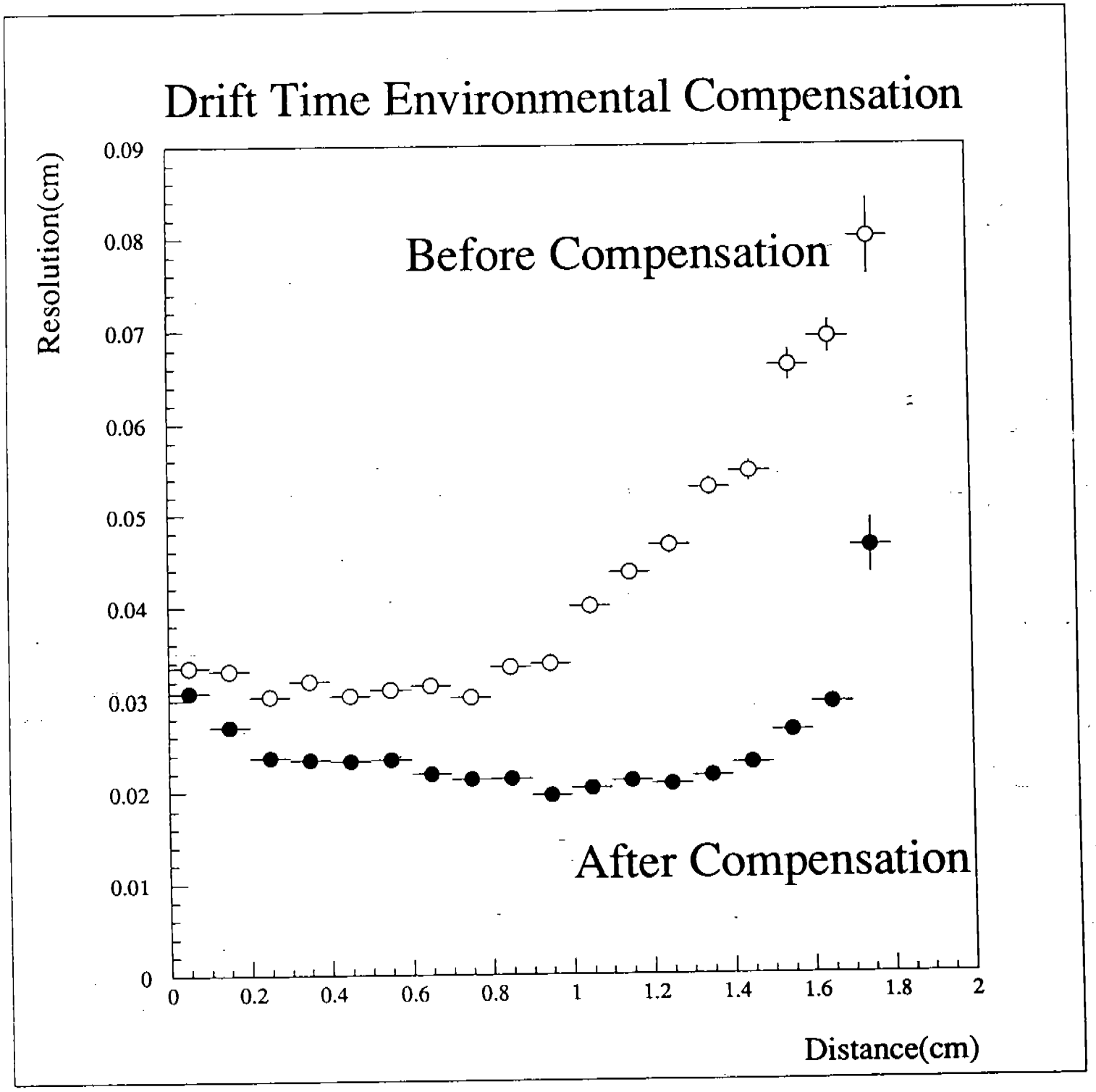
Drift Time Environmental Compensation
Resolution(cm)
0.09
0.08
0.07
0.06
0.05
0.04
0.03
0.02
0.01
0
Before Compensation
After Compensation
0
0.2
0.4
0.6
0.8
1
1.2
1.4
1.6
1.8
2
Distance(cm)

Figure 9.